Document downloaded from:

http://hdl.handle.net/10251/198423

This paper must be cited as:

Paternina-Verona, DA.; Coronado-Hernández, OE.; Fuertes-Miquel, VS. (2022). Numerical modelling for analysing drainage in irregular profile pipes using OpenFOAM. Urban Water Journal. 19(6):569-578. https://doi.org/10.1080/1573062X.2022.2050929

The final publication is available at

https://doi.org/10.1080/1573062X.2022.2050929

Copyright Taylor & Francis

Additional Information

ARTICLE TEMPLATE

Numerical modelling for analysing drainage in irregular profile pipes using OpenFOAM

Duban A. Paternina Verona[a], Oscar E. Coronado-Hernández[b] and Vicente S. Fuertes-Miquel[c]

[a,b]Facultad de Ingeniería, Universidad Tecnológica de Bolívar, Cartagena, Colombia; [c]Departamento de Ingeniería Hidráulica y Medio Ambiente, Universitat Politècnica de València, Valencia, Spain

ARTICLE HISTORY
Compiled February 16, 2022

ABSTRACT
Different methods of two-dimensional and three-dimensional numerical resolution models have been used to predict the air-water interaction in pipe systems in the early 21st century, where reliable and adequate results have been obtained when compared with experimental results. However, the study of the drainage process in pressurized systems with air admitted through openings has not been studied using this type of model due to the complexity that this represents. In this research, a two-dimensional numerical model is developed in the open-source software OpenFOAM; this model represents the drainage of an irregular pipe with air admitted by an air valve, defined by a structured mesh. A validation of the numerical model related to the air admitted by the variation of the air valve diameter is also performed.

KEYWORDS
Drainage, numerical model, admitted air, air valve, Volume of Fraction.

1. Introduction

The drainage of pipeline systems are periodic manoeuvres performed during the maintenance and repair stages of pipe sections and accessories to ensure the adequate transport of water to its destination (Fuertes-Miquel et al. 2019). During the discharge of the water, the air entrapped inside the pipeline systems exhibits thermodynamic behaviour, causing volumetric expansion generated by the absolute pressure drop in the system. This pressure drop can cause collapse of the installation, depending on the height and type of backfill and the stiffness of the pipe (Laanearu et al. 2012; Fuertes-Miquel et al. 2019; Coronado Hernández 2020; Wu et al. 2021). In view of this situation, different failures in pipes and/or pressure conduits due to pressure changes in entrapped air pockets have been reported in the literature, which have led to ruptures, collapse of conduction and sewer systems and failures at the structural level (Espert et al. 1991; Zhou et al. 2002, 2004; Vasconcelos-Neto 2005; Cabrera et al. 2008; Pozos-Estrada et al. 2015). To control negative pressures, air valves are installed, which facilitate rapid draining of the installation (Coronado-Hernández et al. 2017).

CONTACT Duban. A. Paternina Verona. Email: paterninad@utb.edu.co

The numerical resolutions of the 2D and 3D models were used to simulate the hydraulic and thermodynamic behaviour of the water and air phases, respectively (Ho and Riddette 2010; Muralha et al. 2020). Recently, two-dimensional and three-dimensional numerical models that predict pressure patterns and water and air velocities for filling operations in pipes with air valves and for drainage process with entrapped air have been proposed. Liu et al. (2011) created a Volume of Fraction (VOF) model applying a numerical solution for the analysis of overpressures generated in the air entrapped in pipes during the filling processes. Zhou et al. (2011) implemented two-dimensional and three-dimensional numerical models, where each model can adequately reproduce the pressure oscillation patterns by applying the VOF model. Wang et al. (2016) conducted a study to analyse the water-gas separation column, verifying the behaviour based on the cavitation phenomena through velocity contours and vapour volume fraction, applying a two-dimensional numerical resolution. Besharat et al. (2016) compared the results of air pocket overpressures of mathematical models and experimental models with the pressure results of 2D numerical models, in which different mesh structures were applied for comparing convergence criteria of calculations and computational times. Martins et al. (2016) analysed the transient changes in velocity and pressure due to valve closure to evaluate the effects generated by pressure surges using a three-dimensional numerical resolution model. Martins et al. (2017) predicted air pocket pressure and velocity patterns for a pipeline system under rapid filling conditions using three-dimensional numerical models. Besharat et al. (2018) compared experimental results and a mathematical model with a two-dimensional numerical model, analysing air pocket pressure patterns and water drainage velocity associated with an irregular pipe without admitted air, also analysing the impact of the backflow air for different opening degrees of the drainage valves at the discharge points. Besharat et al. (2019) conducted an investigation associated with the analysis of drainage in pipes without admitted air, implementing 2D numerical models, where patterns of air pressure inside the pipe are compared. The results were also used to predict the physical behaviour of the air-water interface during drainage process.

Research associated with the implementation of numerical models for drainage in pipes with admitted air is currently scarce due to the difficulty of proposing numerical solutions that are stable and that guarantee excellent results, in addition to the challenges generated by the simulation of air valves. In this research paper, a two-dimensional numerical model using the open-source software OpenFOAM is proposed to simulate the rapid drainage of an irregular pipe with entrapped air and with an air valve that guarantees the air admitted into the system, with the aim of demonstrating the numerical accuracy of these models under different air pocket size conditions. A change of section is defined for the simulation of the air valve using a geometrical aspect ratio taking into account the two-dimensional conditions (Aguirre-Mendoza et al. 2021). Finally, a validation of the numerical model is performed to determine the influence of the size of the air valve diameter during the drainage process.

2. Materials and methods

For the numerical model, the case of an irregular pipe system composed of a main pipe with diameter equal to 51.4 mm is used as reference. This system is composed of two branches L_1 and L_2, joined together, composed of 1.5 m long sections inclined at 30° with respect to the horizontal axis, which are connected with horizontal pipes with length equal to 1.5 m. The drainage is performed by two pipes with an internal diameter of 23.6 mm and a length of 0.35 m, which at outlets there are two ball valves (V_1 and V_2) with a nominal diameter of 25 mm. At the upstream end, there is an air valve with a known diameter, which admits air into the system (Figure 1).

Five cases where an air valve with an inlet diameter equal to 9.375 mm and different air pocket sizes were considered to evaluate its influence. At the upper end, a pressure transducer was installed, and in the horizontal pipe (right), Ultrasonic Doppler Velocimetry (UDV) was installed to measure the water velocities during the occurrence of the transient phenomenon. Table 1 presents the information of the cases analysed.

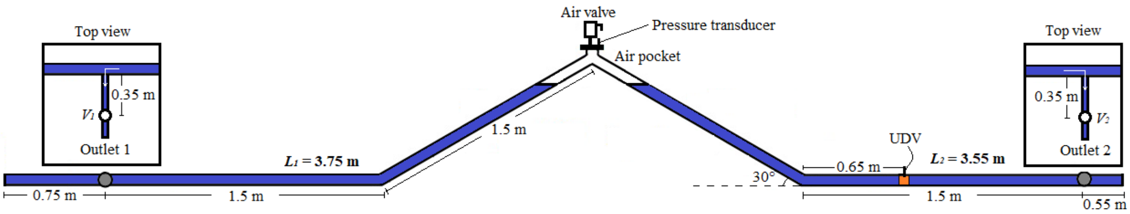

Figure 1. Experimental diagram

Table 1. Specifications of the test cases.

Case	1	2	3	4	5
Air pocket size (m)	null	0.54	0.92	1.32	2.12
Air valve diameter (mm)	9.375	9.375	9.375	9.375	9.375

2.1. *Fundamental equations*

The analysis of the air-water interaction has become a challenge in numerical modelling (Bombardelli 2012; Fuertes-Miquel et al. 2019), considering that air and water have totally different physical and thermodynamic properties (Fuertes 2001). The complexity of analysing the air-water interaction increases considering the changes in flow regimes from laminar to turbulent that occur in the water phase (Ghorai and Nigam 2006; Muralha et al. 2020). The fluids in pipeline systems with air pockets inside and with admitted air are susceptible to abrupt changes in velocity in complex areas, such as contractions and ball valves, which lead to the formation of turbulent processes that are difficult to predict in numerical modelling. During the drainage process, subsonic flow occurs in the air valve. A two-dimensional numerical model has the advantage of quickly simulating the interaction of multiphase (air-water) flows with less computational memory requirement (Zhou et al. 2011; Besharat et al. 2016, 2018).

So it has been an appropriate alternative to develop models that require less computational time. The main challenge of the implementation of the numerical model to represent the drainage of pipes with entrapped air and air valves is the search for the equilibrium between a good approximation of the numerical results to the experimental results and an optimization of the computational time.

The simulation of the drainage process was performed with the open-source software OpenFOAM v1912 using the *compressibleInterFoam* solver. This computational solver is capable of simulating the two fluids (air-water) in the condition of immiscible non-isothermal compressible fluids using a method of interface capturing based on the VOF phase fraction (Hirt and Nichols 1981). The fundamental equations for the solution of the numerical model are the Navier-Stokes equations, which consider a mixed density (ρ_m) and mixed viscosity (μ_m) for each cell analysed (Eqs. (1) and (2)).

$$\nabla \cdot (\rho_m \mathbf{u}) = 0 \tag{1}$$

$$\frac{\partial(\rho_m \mathbf{u})}{\partial t} + \nabla \cdot (\rho_m \mathbf{u}\mathbf{u}) = -\nabla p + \nabla \cdot [\mu_m(\nabla \mathbf{u} + \nabla \mathbf{u}^T)] + \rho_m \mathbf{g} \tag{2}$$

Where $\mathbf{u}$ is the velocity vector, p is the absolute pressure of the fluid, T is the temperature, and $\mathbf{g}$ is the gravitational acceleration vector.

ρ_m and μ_m are defined as a function of the air fraction (α_a). When $\alpha_a = 1.0$, it indicates that the analysed cell is completely filled with air, and when $\alpha_a = 0.0$ it represents the condition of the cell being completely filled with water. Equations for modelling the density and viscosity of a cell are presented below:

$$\rho_m = \alpha_a \rho_a + (1 - \alpha_a)\rho_w \tag{3}$$

$$\mu_m = \alpha_a \mu_a + (1 - \alpha_a)\mu_w \tag{4}$$

Where ρ_a and ρ_w correspond to the densities of air and water, respectively, and μ_a and μ_w to the dynamic viscosities of air and water, respectively.

2.2. *Turbulence model*

The control of turbulence processes has been a complex factor to which several investigations have been dedicated due to the difficulty of predicting turbulence with certainty from a numerical point of view. A numerical model that simulates the behaviour of fluids in a turbulent regime is susceptible to obtaining arbitrary values (Menter 1994). To avoid the problems associated with arbitrary values due to turbulent phenomena, turbulence models are added. To adequately represent the turbulence processes in the numerical model, the k-ω SST turbulence model was used, which merges the best characteristics of the turbulence models of two equations: the k-ϵ model (Launder and Spalding 1983), and the k-ω standart model (Wilcox 1988). This model is suitable in the presence of aerodynamic flows and where adverse pressure gradients are present (Menter 1994, 2009). The turbulence model is represented by the following system of equations:

$$\frac{\partial(\rho k)}{\partial t} + \frac{\partial(\rho u_i k)}{\partial t} = P_k - \beta^* \rho k \omega + \frac{\partial}{\partial x_i}[(\mu + \sigma_k \mu_t)\frac{\partial k}{\partial x_i}] \tag{5}$$

$$\frac{\partial(\rho\omega)}{\partial t}+\frac{\partial(\rho u_i\omega)}{\partial t}=\alpha\frac{1}{\nu_t}P_k-\beta\rho\omega^2+\frac{\partial}{\partial x_i}[(\mu+\sigma_\omega\mu_t)\frac{\partial\omega}{\partial x_i}]+2(1-F_1)\rho\sigma_{w2}\frac{1}{\omega}\frac{\partial k}{\partial x_i}\frac{\partial\omega}{\partial x_i} \quad (6)$$

Where k is the turbulent kinetic energy, ω is the dissipation frequency, F_1 is a blending function, ρ and u_i correspond to the density and velocity of the specific flow, respectively; μ and μ_t correspond to the laminar and turbulent dynamic viscosity, respectively; ν_t is the turbulent kinematic viscosity. The term P_k is given by:

$$P_k=\mu\frac{\partial u_i}{\partial x_j}(\frac{\partial u_i}{\partial x_j}+\frac{\partial u_j}{\partial x_i}) \quad (7)$$

The constants of the turbulence model k-ω SST are arranged through equations with the blending function, as written in the following equations:

$$\alpha=\alpha_1F_1+\alpha_2(1-F_1) \quad (8)$$

$$\beta=\beta_1F_1+\beta_2(1-F_1) \quad (9)$$

$$\sigma_k=\sigma_{k1}F_1+\sigma_{k2}(1-F_1) \quad (10)$$

$$\sigma_\omega=\sigma_{\omega1}F_1+\sigma_{\omega2}(1-F_1) \quad (11)$$

where the constants of the turbulence model k-ω SST according to Menter (2009) are defined with the following values: $\alpha_1=0.555$, $\alpha_2=0.44$, $\beta^*=0.09$, $\beta_1=0.075$, $\beta_2=0.0828$, $\sigma_{k1}=0.85$, $\sigma_{k2}=1.0$, $\sigma_{\omega1}=0.5$, and $\sigma_{\omega2}=0.856$.

The turbulence model works with wall functions for the two variables of the model k-ω SST, These wall functions are adequately adapted for different conditions of the dimensionless distance function ($y+$), and replace the solution of the turbulence models by a semi-empirical formulas based on the wall-law (Spalding 1961; Menter and Esch 2001; Blazek 2015).

2.3. *Numerical schemes*

The numerical modelling schemes were defined through a first-order time discretization, defined and implicit, applying a linear interpolation scheme and a surface normal gradient scheme with non-orthogonal explicit correction for the numerical model. The Gradient and Laplacian schemes were defined based on second-order linear Gaussian integration methods and a second-order undefined-conservative Gaussian scheme, respectively. The Mesh-Wave method was used to calculate the wall distances. The divergence schemes were defined in first-order Gaussian integration methods. Table 2 summarizes the schemes used in the numerical models based on OpenFOAM User Guide Software (Greenshields 2018).

Table 2. Numerical schemes of the model.

Parameters	Schemes	Numerical behavior
Time	Euler	First order, bound, implicit
Gradient	Gauss Linear	Second order, unbounded
Divergence	Gauss Upwind	First order, bound
Laplacian	Gauss Linear	Second order, unbounded
Normal gradient	Corrected	Explicit, non-orthogonal
Interpolation	Linear	Second order, unbounded

2.4. *Mesh and geometric domain*

The mesh is a fundamental component in the solution of the numerical model, which must meet certain physical criteria to ensure a valid solution. The mesh is composed of multiple cells that represent small finite volumes connected by their vertices and faces. The mesh structure will allow the numerical model to define a convergence criterion and a degree of stability from the point of view of spatial discretization.

For the entire geometric domain of the numerical model, a structured mesh was used, which is used in simple geometries to obtain adequate numerical precision. The meshing used should guarantee a reduction in the computational memory required due to structural connectivity between cells and the ease of calculation methods to perform iterative processes (Ali et al. 2017). In the near-wall zone, a gradual refinement was performed to capture with greater accuracy the numerical values generated in the viscous sublayer. Additionally, cells were refined in the areas where abrupt changes in velocity were occurred.

The ball valves V_1 and V_2 were represented by dynamic mesh, through the mesh motion function, which guarantees a rotation defined tabulating the rotation data vs time, considering manual opening of the ball valves during the draining process.

On the other hand, to adequately represent the section changes generated in the air valve and the contraction in the final sections in the two-dimensional numerical model, a slot with geometric aspect ratio was applied between the diameters associated with changes in section and the main diameter of the pipe (Aguirre-Mendoza et al. 2021). This geometrical aspect ratio guarantees an adjustment of the mass flow conditions in a two-dimensional analysis during abrupt section changes such as contractions and expansions. The aspect ratio is represented by the following equation.

$$D_{c,nm} = (\gamma \frac{D_c}{D_p}) D_c \tag{12}$$

Where $D_{c,nm}$ corresponds to the contraction diameter applied to the two-dimensional model. D_c and D_p correspond to the experimental diameters associated with the contraction and the main pipe, respectively. γ is an adjustment factor to adapt the mass flow conditions to the functions of the two-dimensional numerical model. Values of γ between 0.9 and 1.0 guarantee an admissible error in numerical results (Aguirre-Mendoza et al. 2021). A value of 0.95 is used as adjustment factor.

The geometric domain was decomposed into 29909 cells with an average size of 0.003 m. Figure 2 represents the geometric domain of the numerical model and its spatial distribution.

2.5. *Initial and boundary conditions*

It is defined that the numerical model has initial velocity values equal to zero ($u = 0$ m/s) at the inlet, outlet, and walls. The pressure of the air pocket at the inlet and outlet is initially equal to the atmospheric pressure ($p = 101325$ N/m^2), since the system is exposed to the environment. The velocity condition is defined as a function of the absolute pressure in the inlet and outlet, and a noSlip condition in the walls. The pressure conditions at the inlet and outlet work under a function of absolute pressure, which depends on the atmospheric pressure and the pressure exerted by the fluids dynamics, and the pressure condition in the walls is defined as that generated by the displacement of the fluids. The initial temperature of the entire system was $T = 20$°C at room temperature during the experiments. Table 3 details the boundary conditions defined by the OpenFOAM software, which are adequately fit to the experimental conditions.

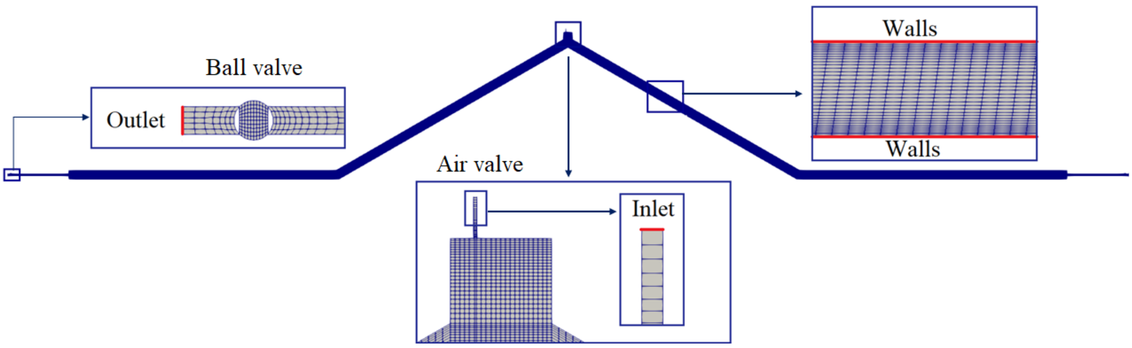

Figure 2. Decomposition of the geometric domain of the two-dimensional numerical model with mesh and boundaries.

Table 3. Boundary Conditions - OpenFOAM.

Variables	Inlet	Outlet	Walls
p (N/m^2)	totalPressure	prghTotalPressure	fixedFluxPressure
u (m/s)	pressureInletOutletVelocity	pressureInletOutletVelocity	noSlip
T (K)	totalTemperature	inletOutlet	zeroGradient
k (m^2/s^2)	turbulentIntensityKineticEnergyInlet	inletOutlet	kqRWallFunction
ω (m^2/s^3)	turbulentMixingLengthFrequencyInlet	inletOutlet	omegaWallFunction

3. Analysis of results and calibration model

The different cases were executed with time steps equal to 0.01 s for a time of 7.0 s. For the simulations, a portable PC with an AMD Ryzen 5 3500U processor with a maximum turbo frequency of 3.7 GHz, 4 cores and 8 threads, and 8 GB of RAM was used. All the cases proposed to evaluate the numerical model that represents the different drainage tests of the irregular pipeline considered fully opened ball valves V_1 and V_2 with gradual and increasing opening. Simultaneously, with an opening time of

1.6 s, the openings of the ball valves allowed drainage at the two ends of the irregular pipe, expansion of the air pocket and admission of air through the air valve.

One of the methodologies for estimating the percentage approximation of the results of the numerical model is the determination of the relative error between the experimental results and the results of the proposed numerical model. For the above, Equation (13) was used.

$$\epsilon_r = |\frac{x_{test} - x_{n.m.}}{x_{test}}| * 100\% \tag{13}$$

Where ϵ_r is the relative error, x_{test} is the value of the experimental test, and $x_{n.m.}$ is the comparative value corresponding to the numerical model. For the determination of the relative error of each test, values of pressure and length of drained water column of the experimental tests was compared with those of the numerical model in different instants of time, with time steps of 0.1 s, and an average relative error was estimated between each measured pattern.

3.1. *Subatmospheric pressures*

Figure 3 shows the pressure patterns obtained from the numerical model for the different cases. The results show an adequate fit of the numerical models with the respective tests, with relative errors between 0.07% and 0.17% (Table 4), where the minimum subatmospheric pressure heads are between 10.15 and 10.29 m. Figure 3a shows that Case 1 (null air pocket size) reaches a minimum absolute pressure of 10.15 m at a time of 1.66 s. Subsequently, due to the action of the admitted air, the absolute pressure pattern begins to increase gradually until reaching the atmospheric condition again. Figure 3e shows the comparison of the pressure patterns of the experimental test and the numerical model corresponding to Case 5, where the subatmospheric pressure head reaches a minimum value of 10.29 m in a time of 1.66 s. The pressure differences occur inversely as the size of the initial air pocket changes in the different cases, where the smaller air pocket generates greater air pressure differences of the air pocket. This pressure drop during the opening times of the ball valves in each case was linear due to the effects generated by the manual opening of ball valves V_1 and V_2.

Table 4. Relative error of pressure patterns results (Tests vs. Numerical Models).

Case	1	2	3	4	5
ϵ_r	0.10%	0.08%	0.17%	0.12%	0.07%

3.2. *Drainage velocity of water columns*

Figure 4 shows that the numerical values of the model do not fit adequately during the initial time, corresponding to the opening time of the ball valves. This is because, in the experimental measurements, the UDV had deficiencies in detecting the displacement of water during drainage; however, from a time of 1.6 s to complete drainage, the results of the numerical model fit appropriately to those obtained experimentally. The drainage velocities of the numerical model reached peak values between 0.18 and 0.41 m/s between 1.66 and 1.68 s.

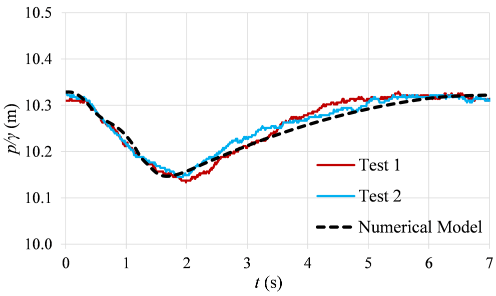

(a) Case 1

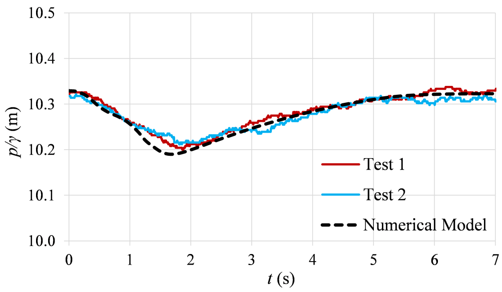

(b) Case 2

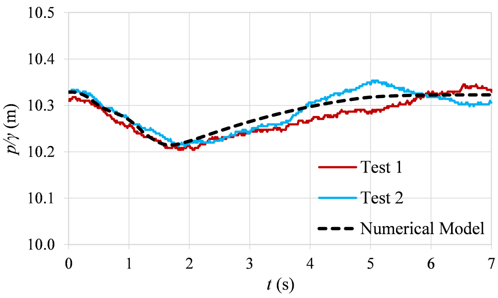

(c) Case 3

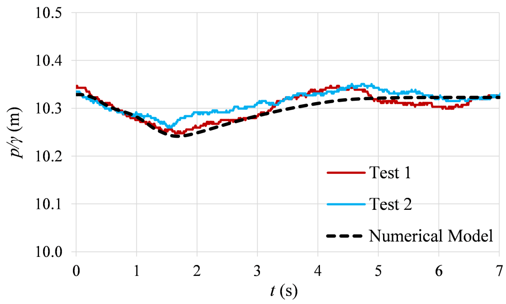

(d) Case 4

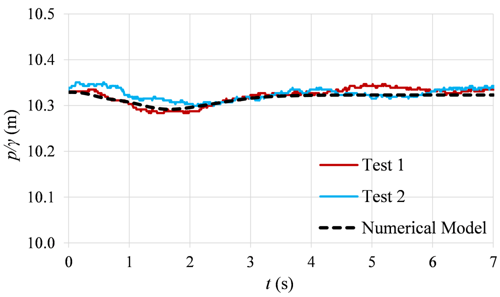

(e) Case 5

Figure 3. Comparison of pressure patterns for Cases 1 to 5.

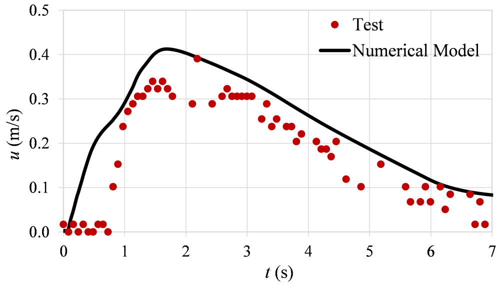

(a) Case 1

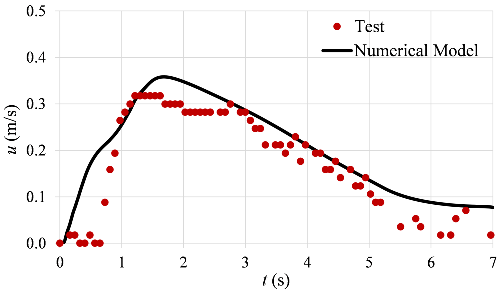

(b) Case 2

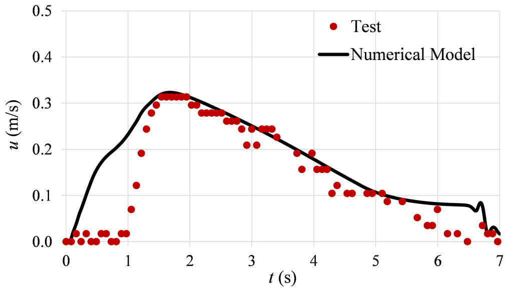

(c) Case 3

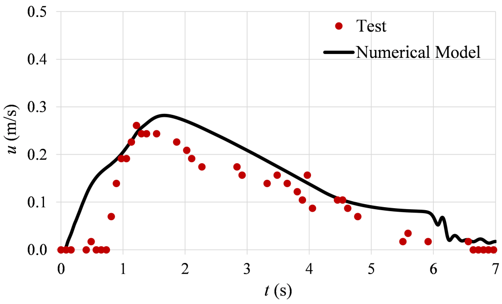

(d) Case 4

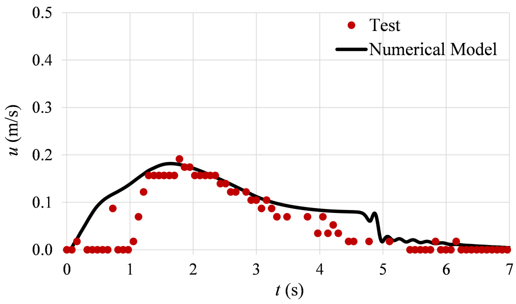

(e) Case 5

Figure 4. Comparison of velocity patterns for Cases 1 to 5.

3.3. *Water column length*

Figure 5 shows the variation in the length of water columns 1 and 2 in the two pipe branches L_1 and L_2, respectively. During the drainage of the water columns, the values of L decrease as a function of time; however, when the water column reaches the horizontal sections, part of the water is retained since the air-water interface in that area is parallel to the axis of the horizontal pipe sections. Overall, drainage in the different cases are adequately associated with the experimental tests with relative errors between 2.1% and 3.7% (Table 5).

Figure 5a shows the displacement of water columns 1 and 2 of Case 1. The water columns decrease, reaching the horizontal sections at 6 s each. On the other hand, Figure 5e, corresponding to Case 5, shows that the initial lengths of water columns 1 and 2 are 2.73 and 2.53 m, respectively, where both water columns reach the horizontal sections in 3 s. The simultaneity of the drainage in the two pipe branches is due to the motion of similar meshes that simulate the openings of ball valves V_1 and V_2 in the numerical model.

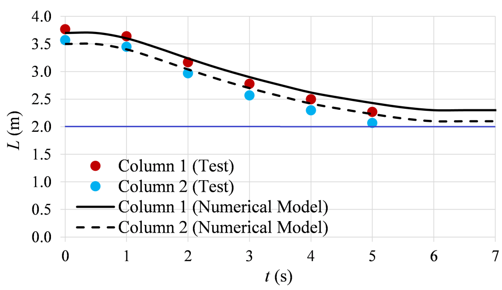

(a) Case 1

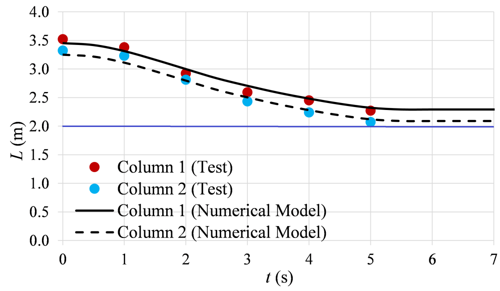

(b) Case 2

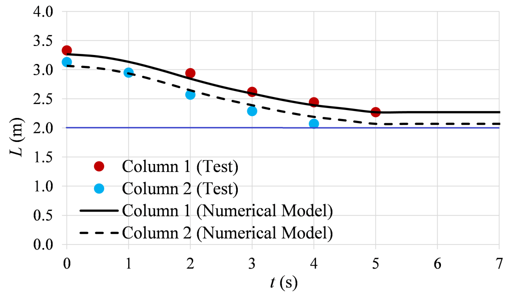

(c) Case 3

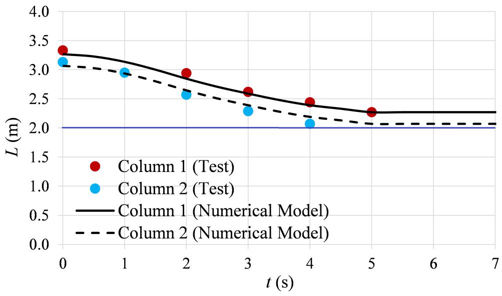

(d) Case 4

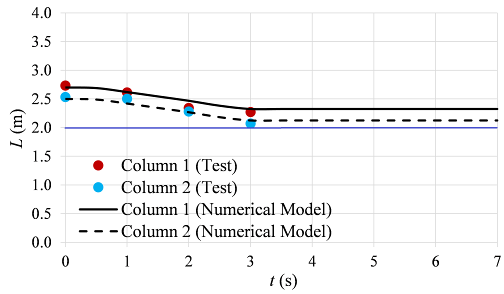

(e) Case 5

Figure 5. Comparison of water column patterns variation for Cases 1 to 5.

Table 5. Relative error of water column length results (Tests vs. Numerical Models).

Case	1	2	3	4	5
ϵ_r	3.7%	2.3%	2.7%	2.1%	2.1%

4. Validation of the numerical model

To demonstrate the robustness of the numerical model, a sixth case (Case 6) was simulated for an air valve with a diameter of 3.175 mm, which was not calibrated during the simulations. Case 6 has an initial air pocket of 0.92 m (equal to the air pocket size of Case 3) to compare the pressure patterns. To simulate Case 6, the dimensions corresponding to the inlet of the air admitted within the geometric domain were adjusted. Figure 6 shows that the pressure pattern results of the numerical model of Case 6 fit adequately to the experimental test, with a relative error in the numerical results of 0.22%.

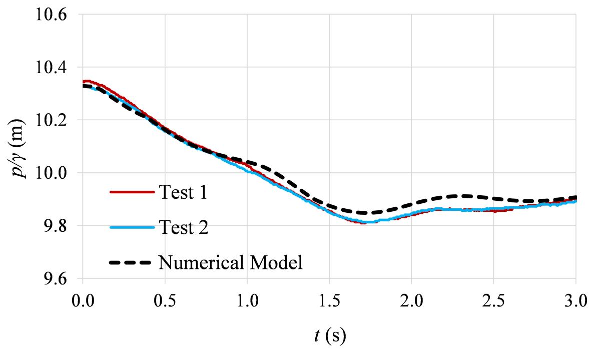

Figure 6. Comparison of the pressure patterns of Case 6.

From a physical point of view, the absolute pressure of the air pocket reaches a minimum value of 9.85 m in 1.66 s; subsequently, there are slight oscillations in the pressure of the air pocket, with a recovery of pressure in the following seconds. This numerical model associated with Case 6 has a smaller-diameter air valve than Cases 1 to 5, which generates critical subatmospheric pressures, and consequently, a slowing of the emptying process.

Case 6 with an air valve of diameter equal to 3.175 mm was simulated under the same conditions of initial air pocket size (0.92 m), degree and opening time of ball valves similar to Case 3, which has an air valve with a diameter of 9.375 mm. Figure 7 clearly shows the air-water interaction in the drainage process at different instants of time for Cases 3 and 6, where it is shown that the displacement of the water columns is faster in Case 3 than in Case 6.

It is important to highlight the importance of air valve diameter size. Good sizing of the air admission devices directly influences the control of the thermodynamic process of air pocket expansion and the mitigation of subatmospheric pressures. Additionally, it was possible to demonstrate the influence of the pressure of the air pocket on the drainage velocity of the water columns since the displacement of the water phase is directly related to the pressure conditions of the air pocket as it is considered a compressible fluid.

5. Conclusions

The two-dimensional numerical model adequately simulated the air-water interaction in the drainage processes of an irregular pipe with air admitted under different air pocket sizes and for air valve diameters (3.175 and 9.375 mm). Each modelled case

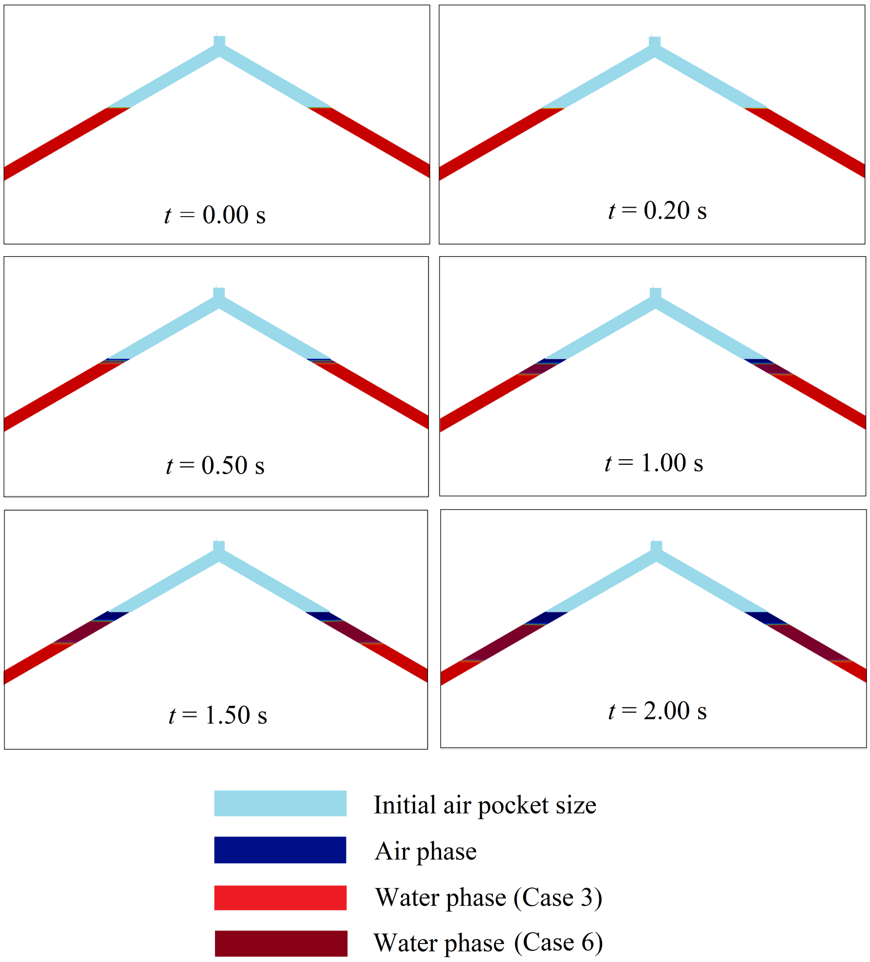

Figure 7. Contours of the air-water interaction - Case 3 vs. Case 6.

adequately predicts its respective experimental tests, obtaining appropriate relative errors for the validation of its numerical results. Controlling air admitted through the air valves in the numerical model influenced the rapid expansion of the air pocket and the progressive recovery of the pressure of the air pocket, and it leads to rapid drainage of the irregular pipeline. Controlling drainage rate and the subatmospheric pressure patterns are influenced by the adequate sizing of the opening diameter of the air valve.

The two-dimensional numerical model allows a simplified analysis that guarantees less computational time and good numerical approximations. The use of the $compressibleInterFoam$ solver in the OpenFOAM software was adequate to analyse the water-air interaction process by considering air and water as compressible fluids, a condition that resembles real conditions. On the other hand, the k-ω SST turbulence model was properly adjusted for the analysis of the air-water interaction in near and far-wall zone of the two-dimensional numerical model and in the air valve where vortices occur due to the phenomenon of turbulence due to the admitted air. Based on the above, the following points associated with the aspects of the numerical model can be concluded:

- Two-dimensional numerical resolution models are a useful alternative in the analysis of drainage processes in pipeline systems with admitted air, allowing adequate results to be obtained.
- The simulation of the admitted air in numerical resolution models that simulate emptying pipes requires adequate turbulence models that adjust to the presence of subsonic aerodynamic flows.
- The air-water interaction can be visualized in detail for the different admitted air conditions associated with the different air valves, where it is shown that the drainage process tends to be slower for air valves with smaller intake diameters.

Nomenclature/Notation

$D_{c,nm}$	= contraction diameter - numerical model (m)
D_c	= contraction diameter - experimental test (m)
D_p	= main pipe diameter - experimental test (m)
F_1	= blending function (-)
$\mathbf{g}$	= gravitational acceleration vector (m/s^2)
k	= turbulent kinetic energy (m^2/s^2)
L	= length of water column (m)
L_1	= pipe branch - left
L_2	= pipe branch - right
P_k	= shear stress (Pa)
p	= absolute pressure (N/m^2)
T	= temperature (°C)
t	= time (s)
$\mathbf{u}$	= velocity vector (m/s)
u	= velocity (m/s)
V_1	= ball valve - left
V_2	= ball valve - right
y^+	= distance function (–)
α_a	= fraction of air volume (–)
γ	= unit weight of water (N/m^3)
ϵ_r	= relative error (%)
μ	= dynamic viscosity (Ns/m^2)
ν	= kinematic viscosity (m^2/s)
ρ	= density (kg/m^3)
ω	= dissipation frequency (1/s)

Subscripts

i	= refers to the spatial component in i
j	= refers to the spatial component in j
a	= refers to air (e.g., air density)
w	= refers to water (e.g., water density)
m	= refers to the mixture between air and water (e.g., mixed density)
t	= refers to a turbulent condition (e.g., turbulent dynamic viscosity)

References

Aguirre-Mendoza, A. M., S. Oyuela, H. G. Espinoza-Román, O. E. Coronado-Hernández, V. S. Fuertes-Miquel, and D. A. Paternina-Verona (2021). 2d cfd modeling of rapid water filling with air valves using openfoam. *Water 13*(21).

Ali, Z., P. G. Tucker, and S. Shahpar (2017). Optimal mesh topology generation for cfd. *Computer Methods in Applied Mechanics and Engineering 317*, 431–457.

Besharat, M., O. E. Coronado-Hernández, V. S. Fuertes-Miquel, M. T. Viseu, and H. M. Ramos (2018). Backflow air and pressure analysis in emptying a pipeline containing an entrapped air pocket. *Urban Water Journal 15*(8), 769–779.

Besharat, M., O. E. Coronado-Hernández, V. S. Fuertes-Miquel, M. T. Viseu, and H. M. Ramos (2019). Computational fluid dynamics for sub-atmospheric pressure analysis in pipe drainage. *Journal of Hydraulic Research 58*(4), 553–565.

Besharat, M., R. Tarinejad, and H. M. Ramos (2016). The effect of water hammer on a confined air pocket towards flow energy storage system. *Journal of Water Supply: Research and Technology—AQUA 65*(2), 116–126.

Blazek, J. (2015). *Computational fluid dynamics: principles and applications*. Butterworth-Heinemann.

Bombardelli, F. (2012). Computational multi-phase fluid dynamics to address flows past hydraulic structures. In *Proceedings of the 4th IAHR International Symposium on Hydraulic Structures, Porto, Portugal*, pp. 9–11.

Cabrera, E., R. Dolz, J. Izquierdo, A. Barbany, L. Onaindia, and J. Villaroel (2008). Transient analysis and waterhammer proteccion. a case study. *Technical report, Eurostudios. Consulting Engineers., Madrid, Spain 1*, 2.

Coronado Hernández, Ó. E. (2020). *Transient phenomena during the emptying process of water in pressurized pipelines*. Ph. D. thesis, Universitat Politècnica de València.

Coronado-Hernández, O. E., V. S. Fuertes-Miquel, M. Besharat, and H. M. Ramos (2017). Experimental and numerical analysis of a water emptying pipeline using different air valves. *Water 9*(2), 98.

Espert, V., E. Cabrera, E. Martínez, R. Pérez, and A. Vela (1991). Air vessel collapse due to a thermal change. a case study. In *Hydraulic Transients with Water Column Separation - 9th and Last Round Table of the IARH Group, Valencia, Spain: IAHR.*

Fuertes, V. (2001). Hydraulic transients with entrapped air pockets phd thesis. *Valencia: Department of Hydraulic Engineering, Polytechnic University of Valencia, Editorial Universitat Politècnica de València.*

Fuertes-Miquel, V. S., O. E. Coronado-Hernández, P. L. Iglesias-Rey, and D. Mora-Meliá (2019). Transient phenomena during the emptying process of a single pipe with water–air interaction. *Journal of Hydraulic Research 57*(3), 318–326.

Fuertes-Miquel, V. S., O. E. Coronado-Hernández, D. Mora-Meliá, and P. L. Iglesias-Rey (2019). Hydraulic modeling during filling and emptying processes in pressurized pipelines: a literature review. *Urban Water Journal 16*(4), 299–311.

Ghorai, S. and K. Nigam (2006). Cfd modeling of flow profiles and interfacial phenomena in two-phase flow in pipes. *Chemical Engineering and Processing: Process Intensification 45*(1), 55–65.

Greenshields, C. J. (2018). Openfoam user guide version 6. *The OpenFOAM Foundation*, 237.

Hirt, C. W. and B. D. Nichols (1981). Volume of fluid (vof) method for the dynamics of free boundaries. *Journal of computational physics 39*(1), 201–225.

Ho, D. and K. Riddette (2010). Application of computational fluid dynamics to evaluate hydraulic performance of spillways in australia. *Australian Journal of Civil Engineering 6*(1), 81–104.

Laanearu, J., I. Annus, T. Koppel, A. Bergant, S. Vučković, Q. Hou, A. S. Tijsseling, A. Anderson, and J. M. van't Westende (2012). Emptying of large-scale pipeline by pressurized air. *Journal of Hydraulic Engineering 138*(12), 1090–1100.

Launder, B. E. and D. B. Spalding (1983). The numerical computation of turbulent flows. In *Numerical prediction of flow, heat transfer, turbulence and combustion*, pp. 96–116. Elsevier.

Liu, D., L. Zhou, B. Karney, Q. Zhang, and C. Ou (2011). Rigid-plug elastic-water model for transient pipe flow with entrapped air pocket. *Journal of Hydraulic Research 49*(6), 799–803.

Martins, N. M., J. N. Delgado, H. M. Ramos, and D. I. Covas (2017). Maximum transient pressures in a rapidly filling pipeline with entrapped air using a cfd model. *Journal of Hydraulic Research 55*(4), 506–519.

Martins, N. M., A. K. Soares, H. M. Ramos, and D. I. Covas (2016). Cfd modeling of transient flow in pressurized pipes. *Computers & Fluids 126*, 129–140.

Menter, F. and T. Esch (2001). Elements of industrial heat transfer predictions. In *16th Brazilian Congress of Mechanical Engineering (COBEM)*, Volume 109, pp. 650.

Menter, F. R. (1994). Two-equation eddy-viscosity turbulence models for engineering applications. *AIAA journal 32*(8), 1598–1605.

Menter, F. R. (2009). Review of the shear-stress transport turbulence model experience from an industrial perspective. *International journal of computational fluid dynamics 23*(4), 305–316.

Muralha, A., J. F. Melo, and H. M. Ramos (2020). Assessment of cfd solvers and turbulent models for water free jets in spillways. *Fluids 5*(3), 104.

Pozos-Estrada, O., I. Pothof, O. A. Fuentes-Mariles, R. Dominguez-Mora, A. Pedrozo-Acuña, R. Meli, and F. Peña (2015). Failure of a drainage tunnel caused by an entrapped air pocket. *Urban Water Journal 12*(6), 446–454.

Spalding, D. (1961). A single formula for the law of the wall. *Journal of Applied Mechanics 28*(3), 455–458.

Vasconcelos-Neto, J. G. (2005). *Dynamic approach to the description of flow regime transition in stormwater systems.* Ph. D. thesis.

Wang, H., L. Zhou, D. Liu, B. Karney, P. Wang, L. Xia, J. Ma, and C. Xu (2016). Cfd approach for column separation in water pipelines. *Journal of Hydraulic Engineering 142*(10), 04016036.

Wilcox, D. C. (1988). Reassessment of the scale-determining equation for advanced turbulence models. *AIAA journal 26*(11), 1299–1310.

Wu, G., X. Duan, J. Zhu, X. Li, X. Tang, and H. Gao (2021). Investigations of hydraulic transient flows in pressurized pipeline based on 1d traditional and 3d weakly compressible models. *Journal of Hydroinformatics 23*(2), 231–248.

Zhou, F., F. Hicks, and P. Steffler (2002). Transient flow in a rapidly filling horizontal pipe containing trapped air. *Journal of Hydraulic Engineering 128*(6), 625–634.

Zhou, F., F. Hicks, and P. Steffler (2004). Analysis of effects of air pocket on hydraulic failure of urban drainage infrastructure. *Canadian Journal of Civil Engineering 31*(1), 86–94.

Zhou, L., D.-y. Liu, and C.-q. Ou (2011). Simulation of flow transients in a water filling pipe containing entrapped air pocket with vof model. *Engineering Applications of Computational Fluid Mechanics 5*(1), 127–140.